American Journal of Applied Mathematics
2022; 10(2): 29-42
http://www.sciencepublishinggroup.com/j/ajam
doi: 10.11648/j.ajam.20221002.12
ISSN: 2330-0043 (Print); ISSN: 2330-006X (Online)

On MHD Flow of Non-newtonian Viscoelastic Fluid over a Stretched Magnetized Surface

Golbert Aloliga[1, *], Ibrahim Yakubu Seini[2], Rabiu Musah[2]

[1]Department of Mathematics, C. K. Tedam University of Technology and Applied Sciences, Navrongo, Ghana

[2]Department of Engineering, University for Development Studies, Tamale, Ghana

Email address:

aloligagolbert@gmail.com (G. Aloliga), yakubuseini@yahoo.com (I. Y. Seini), mrabiu@uds.edu.gh (R. Musah)

[*]Corresponding author

To cite this article:

Golbert Aloliga, Ibrahim Yakubu Seini, Rabiu Musah. On MHD Flow of Non-newtonian Viscoelastic Fluid over a Stretched Magnetized Surface. *American Journal of Applied Mathematics*. Vol. 10, No. 2, 2022, pp. 29-42. doi: 10.11648/j.ajam.20221002.12

Received: March 14, 2022; **Accepted**: April 1, 2022; **Published**: April 9, 2022

Abstract: The purpose of this research is to investigate heat and mass transport in a magnetohydrodynamic (MHD) flow of a non-Newtonian viscoelastic fluid on a stretched magnetized surface. The investigations involve modelling the governing partial differential equations with respect to the Cartesian coordinate system. The models are then transformed into a set of coupled ordinary differential equations. Numerical and graphical solutions were obtained using similarity analysis. The effect of the magnetized sheet on the flow behavior; local skin friction, Nusselt, and Sherwood numbers, are presented in tables. It was observed that an enhanced thickening of the thermal boundary layer was due to the induced magnetization of the sheet. This leads to a significant decline in the heat transfer rate. Certain significant discoveries reported in this research discloses that the effect of viscous dissipation and the non-uniform heat transmission have momentous impact in controlling the rate of heat transfer in the boundary layer region. Again, from the outcome of the analysis it is seen that, the effect of appreciating the Soret number or lessening the Dufour number tends to decrease the velocity and temperature profiles while enhancing the concentration dissemination. Magnetizing the surface shows similar effects on the local skin friction, Nusselt number, and Sherwood number. It is concluded that magnetized surfaces significantly influence the rate of cooling and hence the quality of the penultimate product.

Keywords: Non-newtonian, Viscoelastic Fluid, Magnetized Plate, Convective Boundary Condition, Internal Heat Generation

1. Introduction

Non-Newtonian viscoelastic fluid is a fluid characterized with both viscous and elastic behaviour when distorted making the constitutive relations for viscosity more complex. This type of fluid is useful in manufacturing industries as a result of its distinctive viscous and elastic nature. The increasing demand for plastics, rubber, paint, polyurethanes, and many more, the study of viscoelastic materials has become eminent. Generally speaking, magnetohydrodynamic (MHD) flow is the integration of magnetic fields to flow fields aimed at altering the flow conditions.

The study of electrically conducting fluids of viscoelastic in nature flowing on a porous stretching surface and noted the influence of viscoelasticity of the fluid on the flow velocity was pioneered by Anderson [1]. Later Abel, *et al*. [2] examined the effects of ohmic dispersion and viscous of viscoelastic fluid past elastic surfaces. The heat generation and absorption of viscoelastic fluid over a stretched surface was addressed by Hsiao [3]. Then Makukula *et al*. [4] attained a predictable solution using the linearized method on the viscoelastic fluid in a parallel sheet. The combined effect of convection and radiation on the flow of viscoelastic fluids on a sheet in the presence of a magnetic field was examined by Ghosh and Shit [5]. Other related studies are given in references [6-12]. The effects of entropy generation on viscoelastic fluid [13] and third-grade fluid [14] have been examined. Years later, Han *et al*. [15] examined the coupled heat and mass movement in a viscoelastic fluid using the Cattaneo-Christov heat flux model. But Rostami *et al*. [16] used numerical techniques

and semi-analytical methods to analyze the magnetic field effects in double-diffusive viscoelastic fluid. The parallel effects of buoyancy on viscoelastic fluid over a wedge has been examined with the use of the homotopy analysis method (HAM) by Sheikholeslami *et al*. [17]. Similarly, the magnetic field interaction on nanofluid [18] and the heat flux Cattaneo-Christof model for viscoelastic fluids [19] have been reported. The stagnation point flow [20, 21] of MHD viscoelastic fluid was examined using two auxiliary parameters with the homotopy analysis method (HAM) to determine the heat and mass transfer in a two-dimensional steady viscoelastic fluid over a stretched vertical surface. Consequently, Abbasi *et al.* [22] studied the MHD mixed convective flow of viscoelastic fluid over a stretched surface embedded in porous medium with viscous dissipation. Whilst Ganesh *et al*. [23] analyzed the temperature effects on the thermal boundary layer thickness of Oldroyd-B fluid, Gangadhar *et al.* [24] explored the effects of nonlinear thermal radiation on double-diffusive mixed convection flow of viscoelastic nanofluid on a stretched surface using the Runge– Kutta–Fehlberg numerical scheme together with the shooting technique. Again, Kashifi *et al*. [25] investigated the effects of viscous dissipation on Maxwell fluid with Cattaneo-Christof heat flux while Kumar *et al*. [26] employed the Laplace–Fourier transform to analyse the impact of magnetic field on viscoelastic fluid, [27] outlined the influence of thermal radiation and the induced magnetic field on the convection flow of dissipative fluid. Then Ullah *et al*. [28] performed thermal analysis of water, ethylene glycol and water-ethylene glycol as base fluids with aluminum oxide nano-sized solid particle suspensions.

Recently, the effects of entropy generation on a moving viscoelastic nanofluid over a stretched surface [29] and the dissipation of viscoelastic fluid on non-linear surface [30] have been investigated. Other interesting results were made by Gholinia *et al*. [31] and Ogunseye *et al*. [32]. The mixed convection flow of viscoelastic nanofluid over a horizontal circular cylinder with viscous dissipation [33] using the Keller-box method. Then Golbert *et al*. [34] employed the similarity approach to analyse the boundary layer flow of a non-Newtonian Casson fluid over an exponentially stretched magetized surface. While Etwire *et al*. [35] considered the dynamics of oil-based nanofluid on a permeable stretched surface with radiative heat transfer and dissipative energy [36] analysed the time-dependent hydromagnetic flow past a porous vertical surface in with internally generated heat. Similarly Seini *et al.* [37] catalogued the influence of heat transfer on Casson fluids over exponentially stretched porous surfaces. Then Etwire *et al.* [38] examined the effects of thermophoretic transport of Al_2O_3 nanoparticles on viscoelastic flows of oil-based nanofluid on porous surfaces. The influence of heat transfer on a stretching magnetized surfaces has not been reported in the literature to the best knowledge of the authors. The objective of this study is therefore to examine the impact of heat transfer on non-Newtonian viscoelastic fluids on magnetized surfaces.

2. Mathematical Model

We considered an electrically conducting and incompressible viscoelastic fluid along two-dimensionally stretched perpendicular axes. Assume K_0 , to be the viscoelastic parameter with a variable magnetic field $B(x) = B_0 x^{\frac{n-1}{2}}$ normally applied to the surface. We further assumed that the surface was fixed at the origin, with two equal but opposing forces applied along the x-axis with a magnetic field acting normal to the surface. The stretching velocity is $u_w(x) = ax^n$, where the parameters a and n represent some constants. The equations modelling the flow subject to the Boussinesq approximations and the boundary conditions are given in equations (1) – (4).

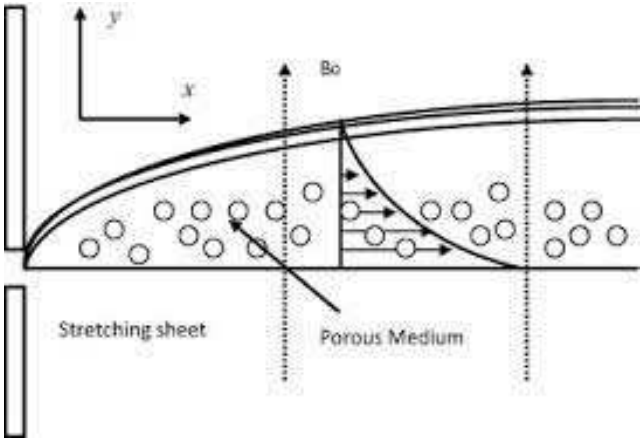

Figure 1. *A flow diagram of the study problem.*

Assuming the x and y-axes acts along the direction and normal to the surface respectively. Further, if the u and v represent the velocity components in the x and y directions respectively, T being the temperature and C, the concentration. The equations modelling flow problem becomes:

$$\frac{\partial u}{\partial x} + \frac{\partial v}{\partial y} = 0 \tag{1}$$

$$u\frac{\partial u}{\partial x} + v\frac{\partial u}{\partial y} = \nu\frac{\partial^2 u}{\partial y^2} + K_0\left[u\frac{\partial^3 u}{\partial x \partial y^2} + v\frac{\partial^3 u}{\partial y^3} + \frac{\partial u}{\partial x}\frac{\partial^2 u}{\partial y^2} - \frac{\partial u}{\partial y}\frac{\partial^2 u}{\partial x \partial y}\right] + g\beta_T(T - T_\infty) + g\beta_C(C - C_\infty) + \frac{\sigma B_0^2 u}{\rho} \tag{2}$$

$$u\frac{\partial T}{\partial x} + v\frac{\partial T}{\partial y} = \alpha\frac{\partial^2 T}{\partial y^2} + \mathcal{V}\left(\frac{\partial u}{\partial y}\right)^2 + \lambda(T^4 - T^4{}_\infty) + \frac{\lambda}{\rho c}(T - T_\infty) + \frac{D_m K_T}{T_m}\frac{\partial^2 C}{\partial y^2} - \frac{\sigma B_0^2 u^2}{\rho} \tag{3}$$

$$u\frac{\partial C}{\partial x} + v\frac{\partial C}{\partial y} = D\left(\frac{\partial^2 C}{\partial y^2}\right) + \frac{D_m K_T}{T_m}\frac{\partial^2 T}{\partial y^2} + \gamma(C - C_\infty) \tag{4}$$

The boundary conditions for the problem are;

$$u = U_0(B)ax^n, v = V_w, T = T_w,\ C = C_w\ at\ y = 0$$

$$u \to 0, \frac{\partial u}{\partial y} \to 0, T \to T_\infty\ C \to C_\infty\ as\ y\ \to \infty \tag{5}$$

3. Similarity Analysis

Introducing the stream function defined as $\psi = \sqrt{avx^{n+1}}f(\eta)$ and a dimensionless variable $\eta = y\sqrt{\frac{ax^{n-1}}{v}}$, the velocity components can be defined in relation to the stream function as;

$$u = \left(\frac{\partial \psi}{\partial y}\right)_x \text{ and } v = \left(\frac{\partial \psi}{\partial x}\right)_y, \tag{6}$$

Equation (6) simplifies to;

$$u = ax^n f', v = -\left\{\frac{n+1}{2}\sqrt{avx^{n-1}}f + \sqrt{avx^{n+1}}.\frac{(n-1)}{2}y\sqrt{\frac{ax^{n-3}}{v}}f'\right\}, \tag{7}$$

Equation (1) is satisfied identically by equation (7).

Introducing the similarity variables, $T = T_o\theta + T_\infty, and\ C\ = (C_w - C_\infty)\phi + C_\infty$, into equations (2), (3), (4), and (5) transform into;

$$f''' - f'^2 + \frac{n+1}{2}ff'' + k_1\left\{(3n-1)f'\mathrm{f}''' + \left(\frac{3n-1}{2}\right)f''^2 - \frac{n+1}{2}\mathrm{f}f^{(4)}\right\} + \mathrm{Gr}\theta + \mathrm{Gm}\phi + M_b f' = 0 \tag{8}$$

$$\frac{1}{Pr}\left(1 - \frac{4}{3}Ra\right)\theta'' + \frac{n+1}{2}f\theta' + Ecf''^2 + Du\phi'' + Q\theta + M_b f'^2 = 0 \tag{9}$$

$$\frac{1}{Sc}\phi'' + \frac{n+1}{2}f\phi' + Sr\theta'' + \lambda\phi = 0 \tag{10}$$

$\mathrm{Gr} = \frac{\mathrm{g}\beta_\mathrm{T}T_0}{\mathrm{a}^2\mathrm{x}^{2\mathrm{n}-1}}$ is Grashof number, $\frac{\mathrm{g}\beta_\mathrm{C}C_0}{\mathrm{a}^2\mathrm{x}^{2\mathrm{n}-1}}$ is the modified Grashof number, $M_b = \frac{\sigma B_0^2}{\mathrm{a}\rho\mathrm{x}^{\mathrm{n}-1}}$ is the bulk magnetic parameter, $\mathrm{k}_1 = \mathrm{k}_0\frac{ax^{n-1}}{v}$ is the viscoelastic parameter, $\lambda = \frac{\gamma}{ax^{n-1}}$ is the reaction rate parameter, $Sr = \frac{D_m K_T}{vT_m}$ is Soret effect parameter, $Sc = \frac{v}{D_m}$ is the Schmidt parameter, $\mathrm{Pr} = \frac{\upsilon}{\alpha}$ represents the Prandtl number, $\mathrm{Ra} = \frac{4\sigma^*\mathrm{T}_\infty^3}{\mathrm{k}\mathrm{K}'}$ represents the thermal radiation parameter, $Du = \frac{D_m K_T C_0}{T_0 v C_s C_p}$ is Duffour number, $Ec = \frac{a^2x^n}{c_p}$ is the Eckert number.

The boundary conditions are transformed as;

At y = 0, $\eta = 0, v = V_w, C = C_w\ and\ T = T_w$

Thus, $f'(0) = 1 - M_s, f(0) = fw, \theta(0) = 1, \phi(0) = 1\ as\ \eta = 0$

$$\text{As } y \to \infty, \eta \to \infty, and\ f'(\infty) \to 0, f''(\infty) \to 0,$$

$$\theta(\infty) \to 0, \phi(\infty) \to 0 \tag{11}$$

Where $fw = \frac{V_w}{\frac{n+1}{2}\sqrt{avx^{n-1}}}$ is the suction parameter and $M_s = \frac{\sigma\overline{B_0}^2}{a\rho/L}$ is the magnetic parameter of the surface.

4. Numerical Procedure

Equations (10), (11), and (12) are the coupled ordinary differential equations whilst equation (13) is the corresponding boundary conditions. These coupled ODEs are of third order and hence complex to solve directly. To acquire a simplified solution, we sort to the order of reduction techniques by letting;

$$f = x_1,\ f' = x_2, f'' = x_3, f''' = x_4, f^{(iv)} = x_5, \theta = x_6, \theta' = x_7, \theta'' = x_8, \phi = x_9, \phi' = x_{10}, \phi'' = x_{11}. \tag{12}$$

Eqns (8) - (10) can then be reduced to first-order ODEs as;

$$x_1' = x_2, \tag{13}$$

$$x_2' = x_3, \tag{14}$$

$$x_3' = x_2^2 - \frac{n+1}{2}(xx_3) - k_1(3n-1)x_2x_4 + \frac{3n-1}{2}x_3^2 - \frac{n+1}{2}xx_5 - Grx_6 - Gmx_9 - M_b x_2, \tag{15}$$

$$x_7' = \frac{1}{\frac{1}{Pr}\left(1+\frac{4}{3}Ra\right)}\left(-\frac{n+1}{2}(x_1x_7) - Ecx_3^2 - Dux_{11} - Qx_6 - M_b x_2^2\right), \tag{16}$$

$$x_{10}' = -Sc\left(Srx_8 + \frac{n+1}{2}(x_1x_{10}) + \lambda x_9\right), \tag{17}$$

The boundary conditions in (1) become;

$$x_2(0) = 1 - M_s, x_1(0) = fw, x_6(0) = 1, x_9(0) = 1, \text{as } \eta = 0,$$
$$x_2(\infty) = 0, x_3(\infty) = 0,\ x_6(\infty) = 0, x_9(\infty) = 0, \text{as } \eta \longrightarrow \infty \tag{18}$$

The MAPLE – 19 software package was implemented and numerical and graphical results are obtained. For the convergence criterion of 10^{-6} a step size of Δh = 0.001 for all the cases was considered. The maximum value of η_∞ to each parameter was known to ensure the correctness of the numerical scheme. We contrast our derived results in relation to the skin-friction coefficient ($f''(0)$) and the local Nusselt number ($-\theta'(0)$) for steady flows. When the values of the unidentified boundary conditions remain unchanged to a final loop, with an error must not more than 10^{-6}.

5. Results and Analysis

The accuracy of the numerical scheme was validated by comparing the results of the analysis to published results of Mohammad *et al*. [20] (Table 1) for varying parameter values. It is observed that the results of the study conformed to three decimal places.

Table 1. *Comparison of values of $f''(0)$ and $-\theta'(0)$ for different values of Pr.*

Pr	[20]		Present work M_s=0, M_b>0		Present work M_s=, M_b=>0	
	$f''(0)$	$-\theta'(0)$	$f''(0)$	$-\theta'(0)$	$f''(0)$	$\theta'(0)$
0.72	0.3064085	3.0276354	0.3064085	3.0276354	0.8701535	5.7757201
0.74	0.3031538	3.0433117	0.3031538	3.0433117	0.8768820	5.8678187
0.76	0.3000066	3.0585296	0.3000066	3.0585296	0.8835089	5.9581408
0.78	0.2969598	3.0733176	0.2969598	3.0733176	0.8900343	6.0467369

5.1. Effects of Parameters on Skin Friction and the Rate of Heat and Mass Transfer with ($M_s > 0$) and (M_b>0)

Table 2 revealed the outcome of varying parameter values with the surface and bulk magnetization of the fluid on the skin friction coefficient, the local Nusselt, and Sherwood numbers. It is detected from the results that the skin friction surges with appreciating values of Pr, Du, Q, Gm, Gr, Ec, and Sc and diminishes with rising values of M_b, M_s, k_1, Sr, λ, fw, Ra and n. This means that the surface magnetic force produces some forces called the Lorenz force on the sheet which causes the local skin friction to decrease. In addition, the results attained by present codes also have been validated by comparing the average Nusselt number with that of the results obtained by Seini *et al*. [37] and Golbert *et al*. [34], is shown in the Table 2. The effects of buoyancy forces, and the chemical species of the fluid are seen to diminish the local skin friction at the plate surface. In the same way, increasing parameter values of Pr, λ, Sc, Du causes higher rate of heat transfer at the plate surface and reduces with increasing values of M_b, M_s, Gm, Gr, Sr k_1, n, Sc, fw, and Gm. Similarly, the mass transfer boosts with increasing values of Ec, Sc, λ, Gr, M_b, M_s and k_1 and decreases with increasing values of Ec, Pr, Ra, fw, Gm, Sr, n, Sc, Gr, and λ.

Table 2. *The results of varying parameter values with the surface and bulk magnetization of the fluid on the local skin friction coefficient, the local Nusselt and Sherwood numbers.*

Pr	λ	Ec	Ra	N	k_1	Sc	fw	Gr	Gm	M_b	M_s	Q	Du	Sr	$f''(0)$	$-\theta'(0)$	$-\phi'(0)$
0.72	2.0	2.0	2.0	1.0	0.1	0.8	0.1	0.1	0.1	0.5	0.5	1.0	2.0	0.1	0.622658	- 2.404953	-3.608115
0.74	2.0	2.0	2.0	1.0	0.1	0.8	0.1	0.1	0.1	0.5	0.5	1.0	2.0	0.1	0.623799	-2.450386	-3.594483
0.76	2.0	2.0	2.0	1.0	0.1	0.8	0.1	0.1	0.1	0.5	0.5	1.0	2.0	0.1	0.624939	- 2.495109	- 3.581246
0.72	2.5	2.0	2.0	1.0	0.1	0.8	0.1	0.1	0.1	0.5	0.5	1.0	2.0	0.1	0.210172	-1.804051	-2.515511
0.72	2.6	2.0	2.0	1.0	0.1	0.8	0.1	0.1	0.1	0.5	0.5	1.0	2.0	0.1	0.306360	-1.846056	-2.583119
0.72	2.0	2.5	2.0	1.0	0.1	0.8	0.1	0.1	0.1	0.5	0.5	1.0	2.0	0.1	0.625528	-2.399031	-3.653745
0.72	2.0	2.6	2.0	1.0	0.1	0.8	0.1	0.1	0.1	0.5	0.5	1.0	2.0	0.1	0.626107	-2.397818	-3.662959
0.72	2.0	2.0	2.5	1.0	0.1	0.8	0.1	0.1	0.1	0.5	0.5	1.0	2.0	0.1	0.610399	-1.888268	-3.772966
0.72	2.0	2.0	3.0	1.0	0.1	0.8	0.1	0.1	0.1	0.5	0.5	1.0	2.0	0.1	0.602009	-1.549680	-3.882144
0.72	2.0	2.0	2.0	2.0	0.1	0.8	0.1	0.1	0.1	0.5	0.5	1.0	2.0	0.1	0.991992	-4.366067	-6.456876
0.72	2.0	2.0	2.0	3.0	0.1	0.8	0.1	0.1	0.1	0.5	0.5	1.0	2.0	0.1	0.515740	-3.041957	-4.393686
0.72	2.0	2.0	2.0	1.0	0.2	0.8	0.1	0.1	0.1	0.5	0.5	1.0	2.0	0.1	0.356840	0.457586	0.607367
0.72	2.0	2.0	2.0	1.0	0.3	0.8	0.1	0.1	0.1	0.5	0.5	1.0	2.0	0.1	0.333034	0.354129	1.039402
0.72	2.0	2.0	2.0	1.0	0.1	0.9	0.1	0.1	0.1	0.5	0.5	1.0	2.0	0.1	0.662369	-2.906232	-4.225794
0.72	2.0	2.0	2.0	1.0	0.1	1.0	0.1	0.1	0.1	0.5	0.5	1.0	2.0	0.1	1.079786	-4.788025	-6.889141
0.72	2.0	2.0	2.0	1.0	0.1	0.8	0.2	0.1	0.1	0.5	0.5	1.0	2.0	0.1	0.558321	-2.240137	-3.387208

Pr	λ	Ec	Ra	N	k_1	Sc	fw	Gr	Gm	M_b	M_s	Q	Du	Sr	$f''(0)$	$-\theta'(0)$	$-\phi'(0)$
0.72	2.0	2.0	2.0	1.0	0.1	0.8	0.3	0.1	0.1	0.5	0.5	1.0	2.0	0.1	0.488212	-2.046088	-3.117004
0.72	2.0	2.0	2.0	1.0	0.1	0.8	0.1	0.2	0.1	0.5	0.5	1.0	2.0	0.1	0.704669	-1.564660	-2.428286
0.72	2.0	2.0	2.0	1.0	0.1	0.8	0.1	0.3	0.1	0.5	0.5	1.0	2.0	0.1	0.794645	-1.144299	-1.861381
0.72	2.0	2.0	2.0	1.0	0.1	0.8	0.1	0.1	0.2	0.5	0.5	1.0	2.0	0.1	0.767337	-1.782065	-2.777938
0.72	2.0	2.0	2.0	1.0	0.1	0.8	0.1	0.1	0.3	0.5	0.5	1.0	2.0	0.1	0.892659	-1.405250	-2.304505
0.72	2.0	2.0	2.0	1.0	0.1	0.8	0.1	0.1	0.1	0.6	0.5	1.0	2.0	0.1	0.648336	-3.114031	-4.603271
0.72	2.0	2.0	2.0	1.0	0.1	0.8	0.1	0.1	0.1	0.7	0.5	1.0	2.0	0.1	0.636323	-3.086750	-5.539359
0.72	2.0	2.0	2.0	1.0	0.1	0.8	0.1	0.1	0.1	0.5	0.6	1.0	2.0	0.1	0.735538	-2.681377	-4.084397
0.72	2.0	2.0	2.0	1.0	0.1	0.8	0.1	0.1	0.1	0.5	0.7	1.0	2.0	0.1	0.713053	-2.118483	-4.327550
0.72	2.0	2.0	2.0	1.0	0.1	0.8	0.1	0.1	0.1	0.5	0.5	2.0	2.0	0.1	0.681704	-2.236629	-4.756745
0.72	2.0	2.0	2.0	1.0	0.1	0.8	0.1	0.1	0.1	0.5	0.5	3.0	2.0	0.1	0.716115	-1.963942	-5.552485
0.72	2.0	2.0	2.0	1.0	0.1	0.8	0.1	0.1	0.1	0.5	0.5	1.0	2.1	0.1	0.628577	-2.534362	-3.601523
0.72	2.0	2.0	2.0	1.0	0.1	0.8	0.1	0.1	0.1	0.5	0.5	1.0	2.2	0.1	0.634468	-2.663048	-3.594815
0.72	2.0	2.0	2.0	1.0	0.1	0.8	0.1	0.1	0.1	0.5	0.5	1.0	2.0	0.1	0.547499	-2.016553	-3.072294
0.72	2.0	2.0	2.0	1.0	0.1	0.8	0.1	0.1	0.1	0.5	0.5	1.0	2.0	0.3	0.478233	-1.673008	-2.593734

5.2. Effects of Parameters on Skin Friction and the Rate of Heat and Mass Transfer When the Surface Magnetization (M_S=0)

Gangadha *et al*. [24] considers a viscous dissipation with heat transfer. From the above table we see that the present result have a good agreement with that of Gangadha *et al*. [24]. From the above discussion, we can say that the present code is valid for laminar flows, convection flow and heat transfer on stretching surfaces. It is discovered from Table 3 that increasing values of Ec, fw, Gr, Gm, Du and λ increase the skin friction and decreases with increasing values of Pr, M_b, Ra, n, Sc, k_1 Sr and fw. This ascertains that the combined effect of soaring thermal diffusion above mass diffusion and the magnetic force, induced Lorenz force to decrease the local skin friction as well as the viscoelastic parameter of the fluid with the suction parameter also decrease the local skin friction at the surface of the plate. Similarly, increasing the parameter values of Pr, λ, Du, Ec, fw, and M_b enhance the rate of heat transfer at the plate surface and reduce with increasing values of Gm, Q, Ra, n, Gr, Sc, and Sr. Moreover, it is observed that the rate of mass transfer increases with increasing values of Sc, fw and Ra; and decreases with increasing values of Pr, λ, Sc, Ec, Sr, Du, Gm, k_1, and Gr.

Table 3. *Results of skin friction coefficient [$f''(0)$], Nusselt [$-\theta'(0)$] and Sherwood numbers [$-\phi'(0)$] for various values of controlling parameters when $M_s = 0$.*

Pr	λ	Ec	Ra	N	k_1	Sc	Fw	Gr	Gm	M_b	Q	Du	Sr	$f''(0)$	$\theta'(0)$	$\phi'(0)$
0.72	2.0	2.0	2.0	1.0	0.1	0.8	0.1	0.1	0.1	0.5	1.0	2.0	0.1	0.863020	6.515995	9.384654
0.74	2.0	2.0	2.0	1.0	1.0	0.8	0.1	0.1	0.1	0.5	1.0	2.0	1.0	0.868898	6.630029	9.361931
0.76	2.0	2.0	2.0	1.0	1.0	0.8	0.1	0.1	0.1	0.5	1.0	2.0	1.0	0.874725	6.742466	9.340368
0.72	2.1	2.0	2.0	1.0	1.0	0.8	0.1	0.1	0.1	0.5	1.0	2.0	1.0	0.963809	7.332090	10.415228
0.72	2.3	2.0	2.0	1.0	1.0	0.8	0.1	0.1	0.1	0.5	1.0	2.0	1.0	1.062447	8.182479	11.477866
0.72	2.0	3.0	2.0	1.0	1.0	0.8	0.1	0.1	0.1	0.5	1.0	2.0	1.0	0.874105	6.503541	9.602169
0.72	2.0	4.0	2.0	1.0	1.0	0.8	0.1	0.1	0.1	0.5	1.0	2.0	1.0	0.885184	6.487116	9.823133
0.72	2.0	2.0	3.0	1.0	1.0	0.8	0.1	0.1	0.1	0.5	1.0	2.0	1.0	0.768494	4.437635	10.044603
0.72	2.0	2.0	4.0	1.0	1.0	0.8	0.1	0.1	0.1	0.5	1.0	2.0	1.0	0.743926	3.473487	10.668501
0.72	2.0	2.0	2.0	2.0	1.0	0.8	0.1	0.1	0.1	0.5	1.0	2.0	1.0	0.288992	5.896937	8.405511
0.72	2.0	2.0	2.0	3.0	1.0	0.8	0.1	0.1	0.1	0.5	1.0	2.0	1.0	-0.190593	3.759988	5.506164
0.72	2.0	2.0	2.0	1.0	0.2	0.8	0.1	0.1	0.1	0.5	1.0	2.0	1.0	0.694800	6.868447	9.792148
0.72	2.0	2.0	2.0	1.0	0.3	0.8	0.1	0.1	0.1	0.5	1.0	2.0	1.0	0.579182	7.119236	10.101729
0.72	2.0	2.0	2.0	1.0	1.0	0.9	0.1	0.1	0.1	0.5	1.0	2.0	1.0	1.386474	9.226351	13.067029
0.72	2.0	2.0	2.0	1.0	1.0	1.0	0.1	0.1	0.1	0.5	1.0	2.0	1.0	1.353231	10.134442	14.014673
0.72	2.0	2.0	2.0	1.0	1.0	0.8	0.2	0.1	0.1	0.5	1.0	2.0	1.0	0.698437	6.395024	9.431744
0.72	2.0	2.0	2.0	1.0	1.0	0.8	0.3	0.1	0.1	0.5	1.0	2.0	1.0	1.212693	8.395394	12.620778
0.72	2.0	2.0	2.0	1.0	1.0	0.8	0.1	0.2	0.1	0.5	1.0	2.0	1.0	0.864157	4.074335	5.873071
0.72	2.0	2.0	2.0	1.0	1.0	0.8	0.1	0.3	0.1	0.5	1.0	2.0	1.0	0.901197	2.954986	4.279385
0.72	2.0	2.0	2.0	1.0	1.0	0.8	0.1	0.1	0.2	0.5	1.0	2.0	1.0	0.997634	4.651584	6.790292
0.72	2.0	2.0	2.0	1.0	1.0	0.8	0.1	0.1	0.3	0.5	1.0	2.0	1.0	1.098604	3.596174	5.341704
0.72	2.0	2.0	2.0	1.0	1.0	0.8	0.1	0.1	0.1	0.6	1.0	2.0	1.0	0.818757	7.074136	10.077487
0.72	2.0	2.0	2.0	1.0	1.0	0.8	0.1	0.1	0.1	0.7	1.0	2.0	1.0	0.776061	7.637356	10.78073
0.72	2.0	2.0	2.0	1.0	1.0	0.8	0.1	0.1	0.1	0.5	3.0	2.0	1.0	1.525287	7.685032	18.453154
0.72	2.0	2.0	2.0	1.0	1.0	0.8	0.1	0.1	0.1	0.5	4.0	2.0	1.0	1.536952	7.056104	20.10537
0.72	2.0	2.0	2.0	1.0	1.0	0.8	0.1	0.1	0.1	0.5	1.0	3.0	1.0	0.994380	9.446465	9.157849
0.72	2.0	2.0	2.0	1.0	1.0	0.8	0.1	0.1	0.1	0.5	1.0	4.0	1.0	1.127007	12.23834	8.971551
0.72	2.0	2.0	2.0	1.0	1.0	0.8	0.1	0.1	0.1	0.5	1.0	0.2	0.2	0.802787	5.976076	8.710887
0.72	2.0	2.0	2.0	1.0	1.0	0.8	0.1	0.1	0.1	0.5	1.0	0.2	0.3	0.761065	5.548860	8.185215

6. Graphical Results

In this study of hydromagnetic heat and mass transfer flow of viscoelastic fluid flow over a stretching surface, considering the effects of thermal radiation and convection is investigated. Applying numerical parameter values to the problem, we can discuss their effects on the velocity, temperature, and concentration distributions. The importance and practical use of graphical illustration of numerical results cannot be over-emphasized because they give a pictorial view to help discuss the effect of different parameters. The validation of results is done by comparing the results obtained from present code with those of Golbert et al. [34] demonstrated for two different Grashof number, Gr=0.1, and Gm=0.1 in Figure 4 and Figure 3 respectively. Obviously these figures from the obtained results show very good agreement with the previous study.

6.1. The Effects of Varying Parameters on Velocity Profiles

The outcomes of varying the values of parameters on the velocity profiles are revealed in Figures 2-11. The effects of both the magnetic parameter at the surface and the bulk on the velocity are plotted in Figures 9 and 11 respectively. It is observed that the velocity decreases at the surface with increasing the magnetic field intensity. The existence of the magnetic field which opposes the flow slows down the fluid. This claim is confirmed in (Table 2) when M_s varies inversely proportional to the skin friction. Hence, the shear wall stress increases as a result of a drag-like force. An increase in Pr in (Figure 2) increases the kinematic viscosity and consequently reduces the velocity. When the buoyancy forces (λ) increases, the velocity of the fluid accelerates thereby thickening the boundary-layer in Figure 7. It is worth noting that, a better flow kinematics is obtainable by increasing buoyancy forces.

The velocity profiles for various values of the suction parameter (*fw*), are shown in Figure 8. It seen from the figure that surging values of suction decelerates the velocity. The velocity retards because, suction causes resistance to the fluid flow. Figure 11 shows the impact of the visco-elastic parameter k_1 on the velocity profile. We have observed that the axial velocity increases near the stretching sheet with an increase of the visco-elastic parameter (k_1), while near the edge of the boundary layer the reverse process happened. The effect of the Soret number on the velocity field is shown in Figure 6. The Soret number defines the effect of the temperature gradients inducing significant mass diffusion effects. It is noticed that an increase in the Soret number increases the velocity within the boundary layer.

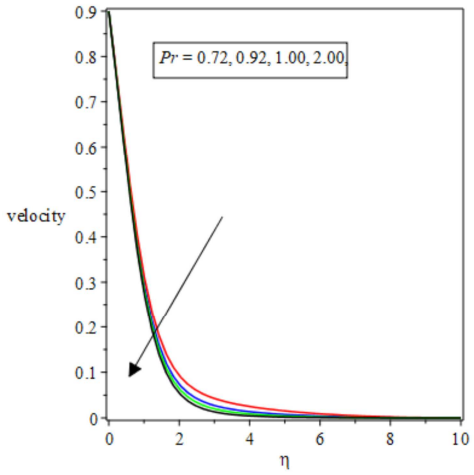

Figure 2. *Effects of Pr on the velocity profile for λ=1, Ec =2, Ra =2, Q =2, n =5, Du = 2, k_1 = 0.1, Sr =2, Sc = 0.5, fw = 0.1, Gr =0.2, Gm =0.2, M_b =0.1 and M_s =0.1.*

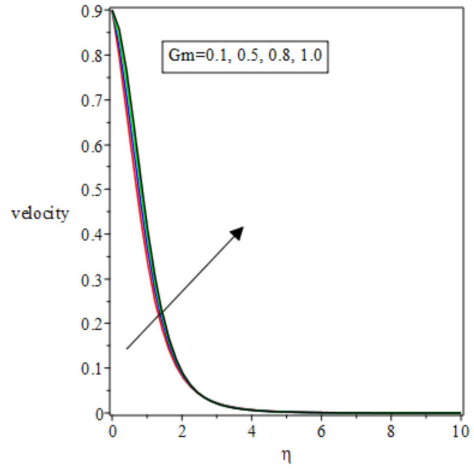

Figure 3. *Effects of Gm on the velocity profile for Pr=0.72, λ=1, Ec =2, Ra =2, Q =2, n =5, Du = 2, k_1 = 0.1, Sr =2, Sc = 0.5, fw = 0.1, Gr =0.1, M_b =0.1 and M_s =0.1.*

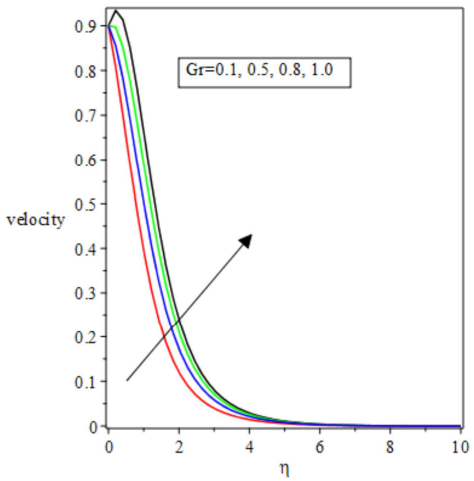

Figure 4. *Effects of Gr on the velocity profile for Pr=0.72, λ=1, Ec =2, Ra =2, Q =2, n =5, Du = 2, k_1 = 0.1, Sr =2, Sc = 0.5, fw = 0.1, Gm =0.1, M_b =0.1 and M_s =0.1.*

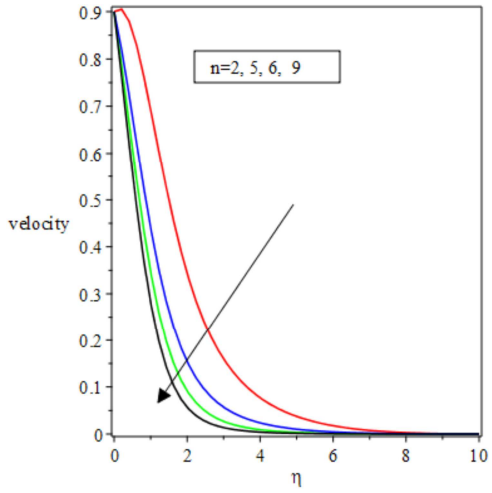

Figure 5. *Effects of n on the velocity profile for Pr=0.72, λ=1, Ec =2, Ra =2, Q =2, Du = 2, k_1 = 0.1, Sr =2, Sc = 0.5, fw = 0.1, Gr =0.1, Gm =0.1, M_b =0.1 and M_s =0.1.*

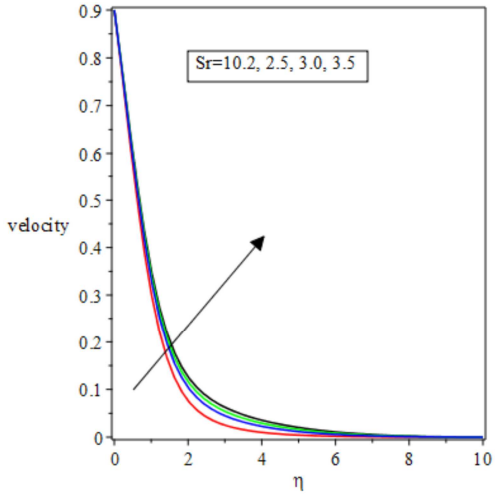

Figure 6. *Effects of Sr on the velocity profile for Pr=0.72, λ=1, Ec =2, Ra =2, Q =2, n =5, Du = 2, k_1 = 0.1, Sc = 0.5, fw = 0.1, Gm=0.1, Gr =0.1, M_b =0.1 and M_s =0.1.*

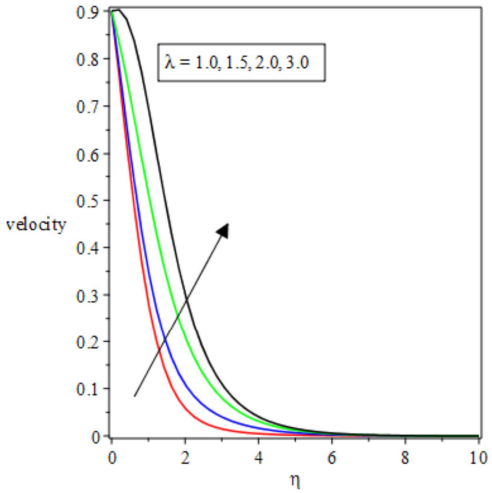

Figure 7. *Effects of λ on the velocity profile for Pr=0.72, Ec =2, Ra =2, Q =2, n =5, Du = 2, k_1 = 0.1, Sc = 0.5, fw = 0.1, Gm=0.1, Gr =0.1, M_b =0.1 and M_s =0.1.*

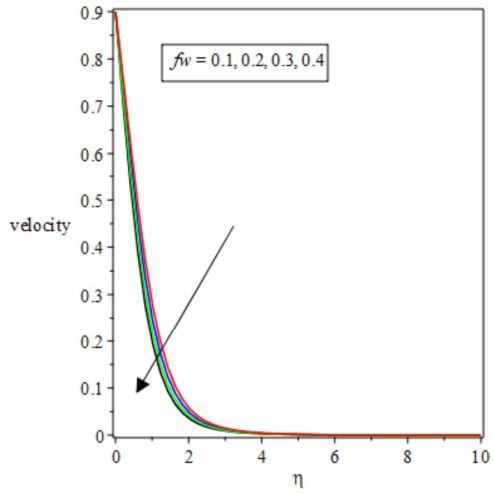

Figure 8. *Effects of fw on the velocity profile for Pr=0.72, Ec =2, λ=1, Ra =2, Q =2, n =5, Du = 2, k_1 = 0.1, Sc = 0.5, Gm=0.1, Gr =0.1, M_b =0.1 and M_s =0.1.*

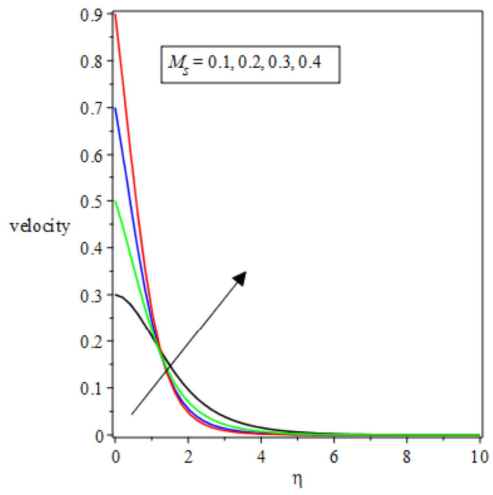

Figure 9. *Effects of M_s on the velocity profile for Pr=0.72, Ec =2, λ=1, Ra =2, Q =2, n =5, Du = 2, k_1 = 0.1, Sc = 0.5, fw = 0.1, Gm=0.1, Gr =0.1 and M_b =0.1.*

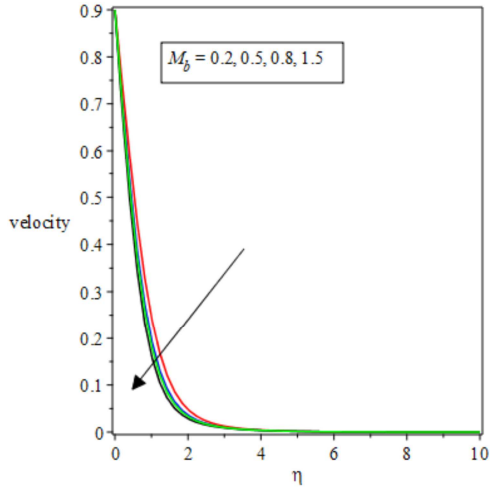

Figure 10. *Effects of M_b on the velocity profile for Pr=0.72, Ec =2, λ=1, Ra =2, Q =2, n =5, Du = 2, k_1 = 0.1, Sc = 0.5, fw = 0.1, Gm=0.1, Gr =0.1 and M_s =0.1.*

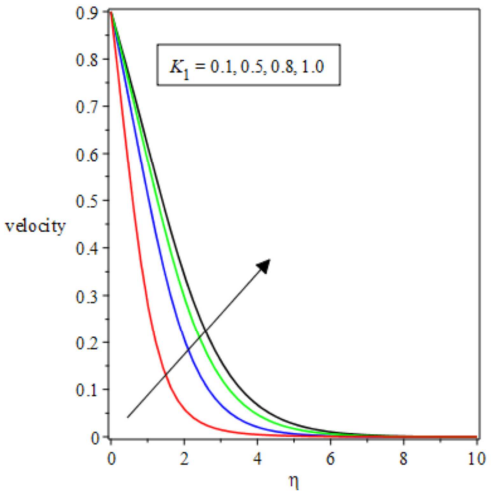

Figure 11. *Effects of k_1 on the velocity profile for Pr=0.72, Ec =2, λ=1, Ra =2, Q =2, n =5, Du = 2, Sc = 0.5, fw = 0.1, Gm=0.1, Gr =0.1, M_s =0.1 and M_b = 0.1.*

6.2. The Effects of Varying Parameters on Temperature Profiles

Figures 12-23 displays the impact of varying parameters on temperature. Figure 12 presents the disparity of Pr on the temperature profiles. Enhancing the Prandtl number deteriorates both the temperature of the fluid and the thickness of the thermal boundary layer. Since the Prandtl number is the ratio of the momentum diffusivity to the thermal diffusivity means an increase in the Prandtl number will decrease the thermal diffusivity or increase the momentum diffusivity. Figure 21 shows the impact of the buoyancy parameter (λ) on the temperature profile. The thermal boundary-layer thickness increases with rising values of the buoyancy parameter. It can be seen in Figure 22 that, greater values of fw reduce the temperature. From figure 18, the thermal radiation is seen to increase with the temperature. This is since as more heat is generated within the fluid, the fluid temperature increases leading to a sharp inclination of the temperature gradient between the plate surface and the fluid. In figures 13 and 15, the impacts of the magnetic parameters M_s and M_b on the temperature distribution curves are shown. The Lorentz force arises due to the magnetic field applied perpendicular to the flow increasing the temperature. The effects of magnetic field on the skin-friction, causes heating thereby increasing temperature at the wall and the thickness of the thermal boundary layer. The effect of heat source parameter Q on the temperature profile is shown in figure 19. From the figure, it is found that the heat source parameter Q increases the conductivity of the fluid and the thickening of the thermal boundary layer. This shows that the thermal boundary layer thickness increases with an increase of the heat source parameter. Figure 17 shows the impact of the visco-elastic parameter k_1 on the temperature profile. Viscoelasticity plays an important role in the boundary layer thickness as the visco-elastic parameter k_1 increases the temperature profile. Figure 23 shows the influence of viscous dissipation parameter Ec on the temperature profile. It is observed that increasing the viscous dissipation parameter Ec increases the temperature profile. This shows that the thermal boundary layer thickness increases with an increase of viscous dissipation parameter Ec.

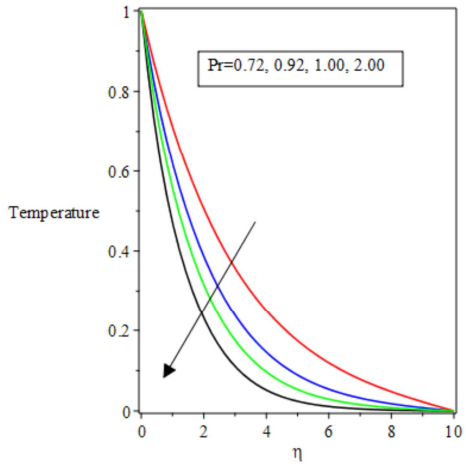

Figure 12. *Effects of Pr on the Temperature profiles for Ec=2, λ=1, Ra =2, n=5, Q =2, Du = 2, k_1 = 0.1, Sr =2, Sc = 0.5, fw = 0.1, Gr =0.1, Gm =0.1, M_b =0.1 and M_s =0.1.*

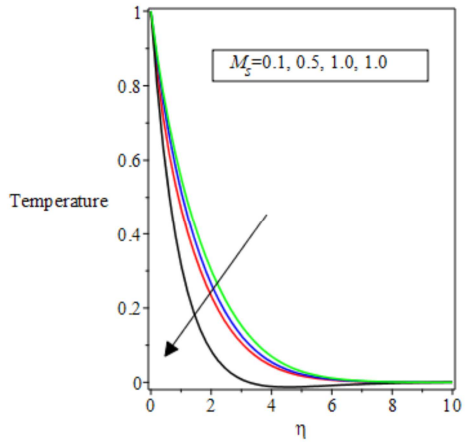

Figure 13. *Effects of M_s on the Temperature profiles for Pr=0.72, Ec=2, λ=1, Ra =2, n=5, Q =2, Du = 2, k_1 = 0.1, Sr =2, Sc = 0.5, fw = 0.1, Gr =0.1, Gm =0.1 and M_b =0.1.*

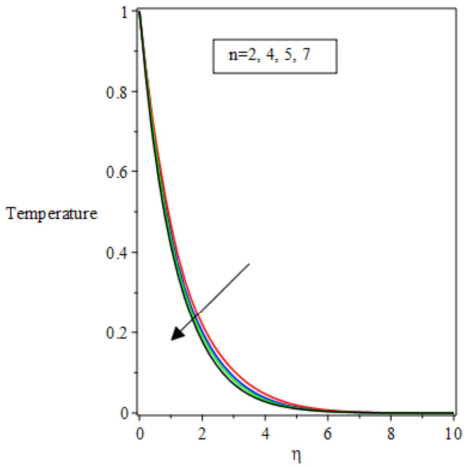

Figure 14. *Effects of n on the Temperature profiles for Pr=0.72, Ec=2, λ=1, Ra =2, Q =2, Du = 2, k_1 = 0.1, Sr =2, Sc = 0.5, fw = 0.1, Gr =0.1, Gm =0., M_b =0.1 and M_s = 0.1.*

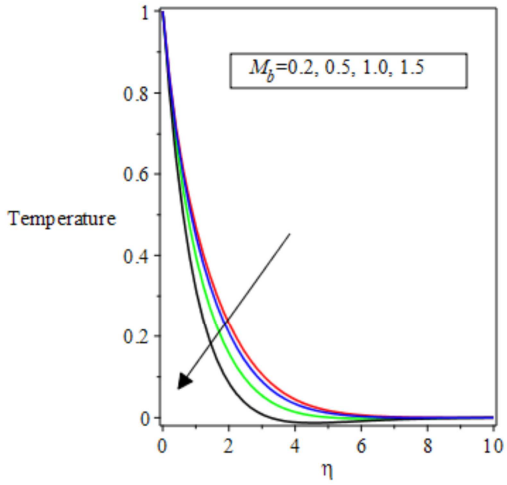

Figure 15. *Effects of M_b on the Temperature profiles for Pr=0.72, Ec=2, λ=1, Ra =2, Q =2, Du = 2, k_1 = 0.1, Sr =2, Sc = 0.5, fw = 0.1, Gr =0.1, Gm =0.1 and M_s = 0.1.*

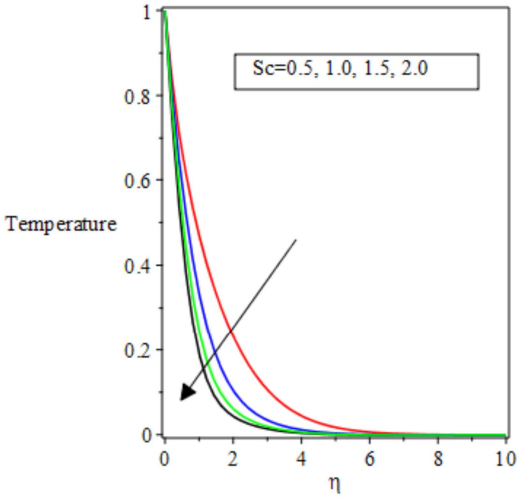

Figure 16. *Effects of Sc on the Temperature profile for Pr=0.72, Ec =2, Ra =2, Q =2, n =5, Du = 2, k_1 = 0.1, Sr =2, λ = 1, fw = 0.1, Gm=0.1, Gr =0.1, M_b =0.1 and M_s =0.1.*

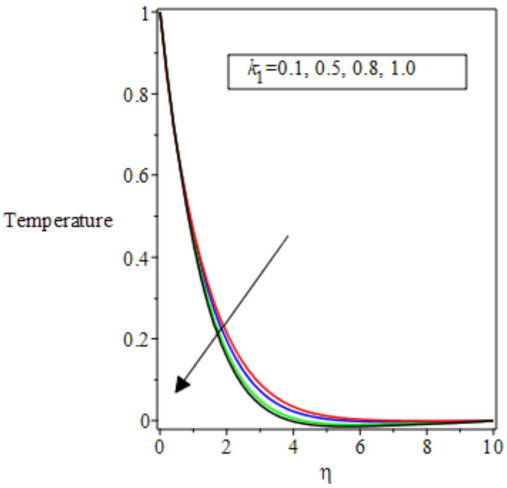

Figure 17. *Effects of k_1 on the Temperature profile for Pr=0.72, Ec =2, Ra =2, Q =2, n =5, Du = 2, Sc= 0.5, Sr =2, λ = 1, fw = 0.1, Gm=0.1, Gr =0.1, M_b =0.1 and M_s =0.1.*

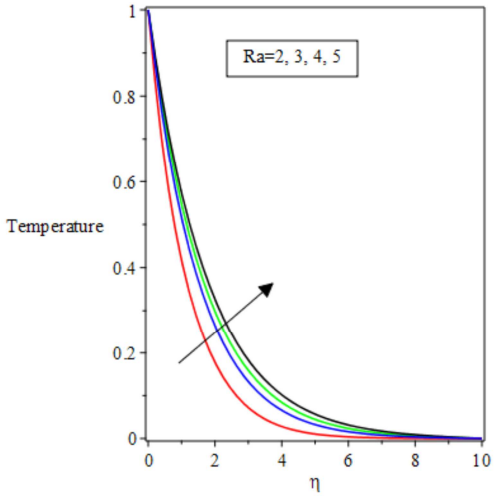

Figure 18. *Effects of Ra on the Temperature profile for Pr=0.72, Ec =2, Q =2, n =5, Du = 2, Sc= 0.5, Sr =2, λ = 1, k_1 = 0.1, fw = 0.1, Gm=0.1, Gr =0.1, M_b =0.1 and M_s =0.1.*

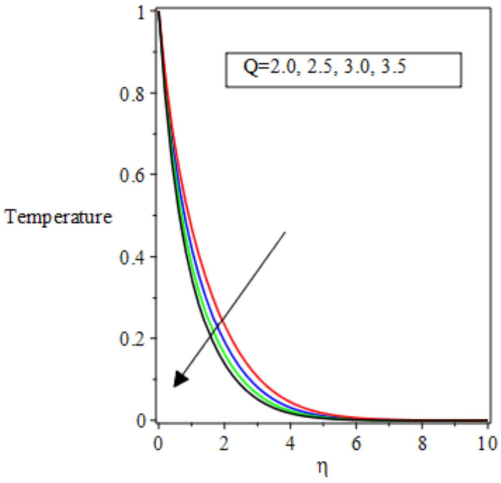

Figure 19. *Effects of Q on the Temperature profile for Pr=0.72, Ec =2, Ra =2, Q =2, n =5, Du = 2, Sc= 0.5, Sr =2, λ = 1, k_1 = 0.1, fw = 0.1, Gm=0.1, Gr =0.1, M_b =0.1 and M_s =0.1.*

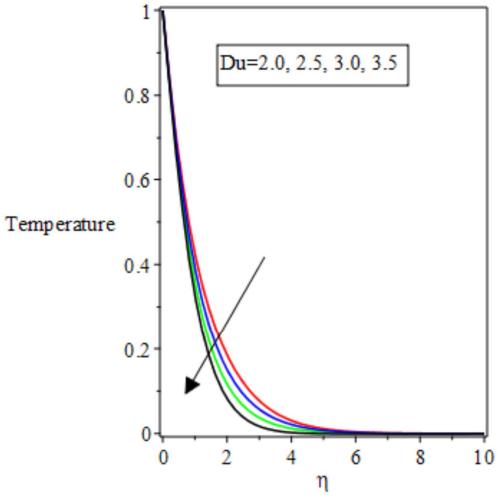

Figure 20. *Effects of Du on the Temperature profile for Pr=0.72, Ec =2, Ra =2, λ=1, Q =2, n =5, k_1 = 0.1, Sr =2, Sc = 0.5, fw = 0.1, Gm=0.1, Gr =0.1, M_b =0.1 and M_s =0.1.*

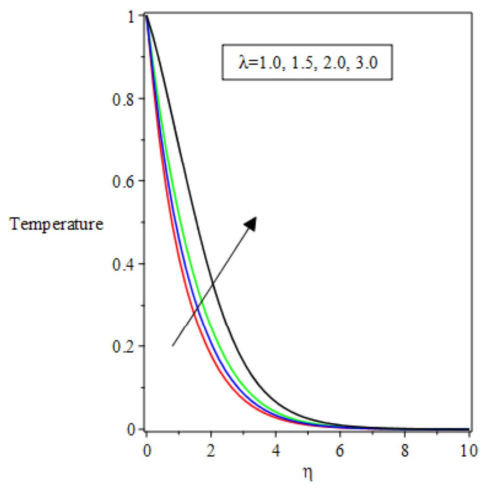

Figure 21. *Effects of λ on the Temperature profile for Pr=0.72, Ec =2, Ra =2, Q =2, n =5, Du = 2, k_1 = 0.1, Sr =2, Sc = 0.5, fw = 0.1, Gm=0.1, Gr =0.1, M_b =0.1 and M_s =0.1.*

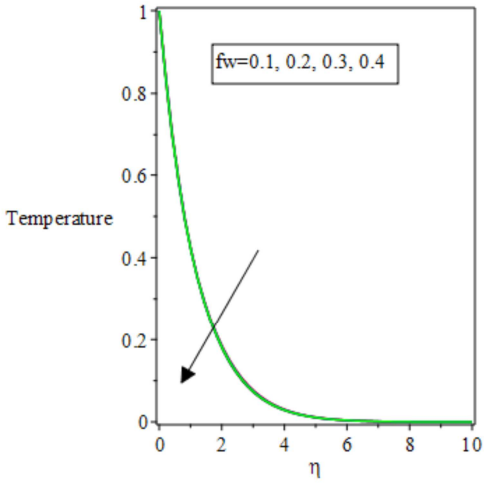

Figure 22. *Effects of fw on the Temperature profile for Pr=0.72, Ec =2, Ra =2, λ=1, Q =2, n =5, Du = 2, k_1 = 0.1, Sr =2, Sc = 0.5, fw = 0.1, Gm=0.1, Gr =0.1, M_b =0.1 and M_s =0.1.*

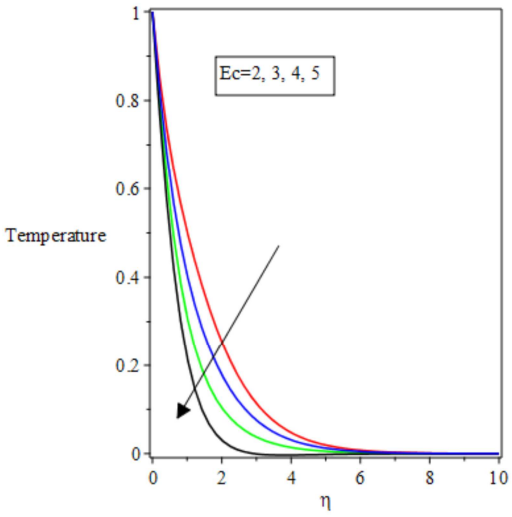

Figure 23. *Effects of Ec on the Temperature profiles for Pr=0.72, λ=1, Ra =2, Q =2, Du = 2, k_1 = 0.1, Sr =2, Sc = 0.5, fw = 0.1, Gr =0.1, Gm =0.1, M_b =0.1 and M_s = 0.2.*

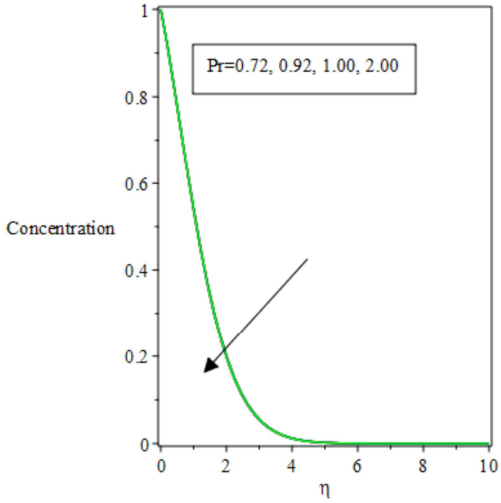

Figure 24. *Effects of Pr on the Concentration profiles for n=5, λ=1, Ec=2, Ra =2, Q =2, Du = 2, = 0.1, Sr =2, Sc = 0.5, fw = 0.1, k_1 = 0.1, Gr =0.1, Gm =0.1, M_b =0.1 and M_s = 0.1.*

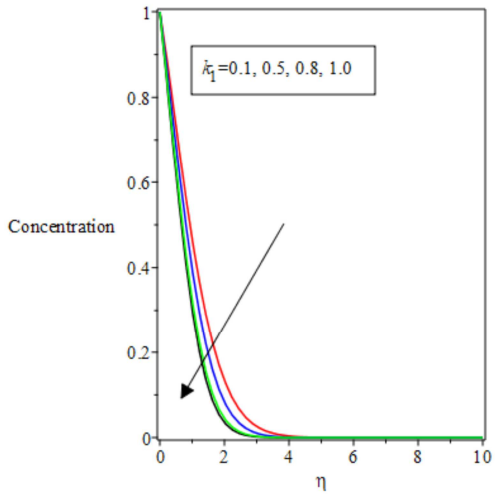

Figure 25. *Effects of k_1 on the Concentration profiles for Pr=0.72, λ=1, Ec=2, Ra =2, Q =2, Du = 2, = 0.1, Sr =2, Sc = 0.5, fw = 0.1, Gr =0.1, Gm =0.1, M_b =0.1 and M_s = 0.1.*

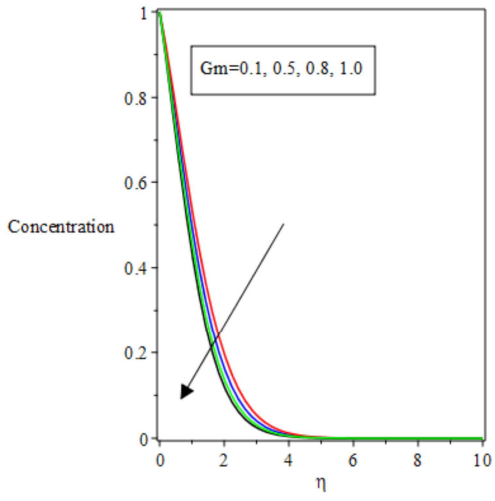

Figure 26. *Effects of Gm on the Concentration profiles for Pr=0.72, λ=1, Ec=2, Ra =2, Q =2, Du = 2, k_1 = 0.1, Sr =2, Sc = 0.5, fw = 0.1, Gr =0.1, Gm =0.1, M_b =0.1 and M_s = 0.1.*

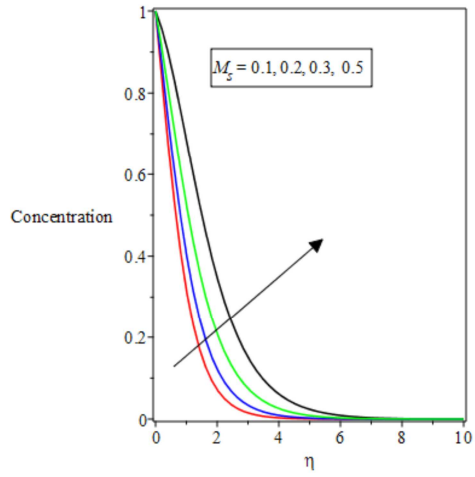

Figure 27. *Effects of M_s on the Concentration profiles for Pr=0.72, λ=1, Ec=2, Ra =2, Q =2, Du = 2, = 0.1, Sr =2, Sc = 0.5, fw = 0.1, $k_1 = 0.1$, Gr =0.1, Gm =0.1 and M_b =0.1.*

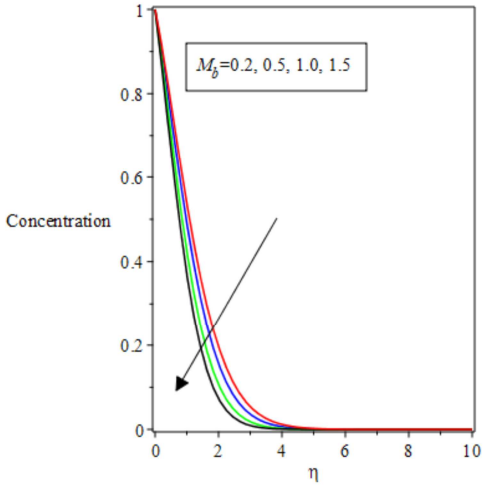

Figure 28. *Effects of M_b on the Concentration profiles for Pr=0.72, λ=1, Ec=2, Ra =2, Q =2, Du = 2, = 0.1, Sr =2, Sc = 0.5, fw = 0.1, $k_1 = 0.1$, Gr =0.1, Gm =0.1 and $M_s = 0.1$.*

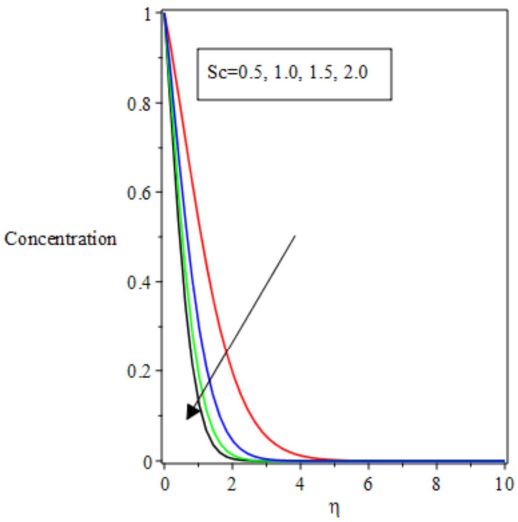

Figure 29. *Effects of Sc on the Concentration profiles for Pr=0.72, λ=1, Ec=2, Ra =2, Q =2, Du = 2, = 0.1, Sr =2, fw = 0.1, $k_1 = 0.1$, Gr =0.1, Gm =0.1, M_b =0.1 and $M_s = 0.1$.*

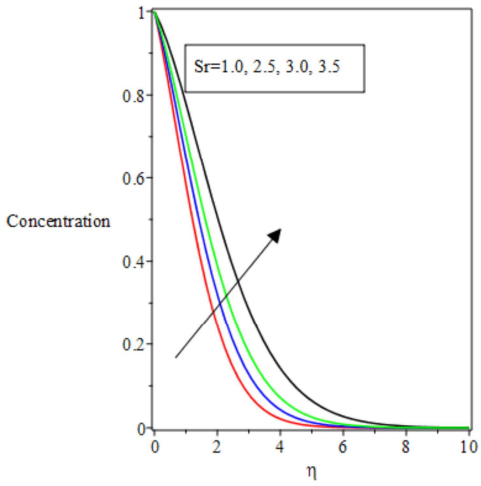

Figure 30. *Effects of Sr on the Concentration profiles for Pr=0.72, λ=1, Ec=2, Ra =2, Q =2, Du = 2, = 0.1, Sc = 0.5, fw = 0.1, $k_1 = 0.1$, Gr =0.1, Gm =0.1, M_b =0.1 and $M_s = 0.1$.*

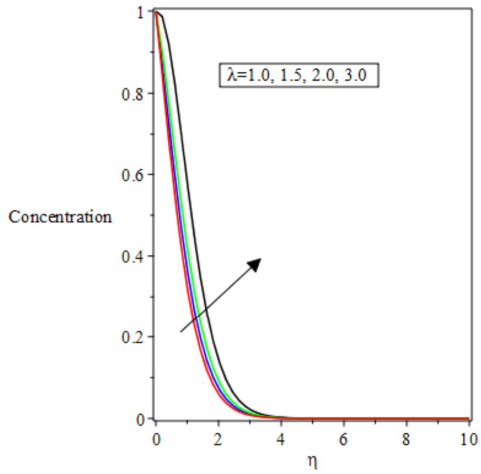

Figure 31. *Effects of λ on the Concentration profiles for Pr=0.72, Ec=2, Ra =2, Q =2, Du = 2, = 0.1, Sr =2, Sc = 0.5, fw = 0.1, $k_1 = 0.1$, Gr =0.1, Gm =0.1, M_b =0.1 and $M_s = 0.1$.*

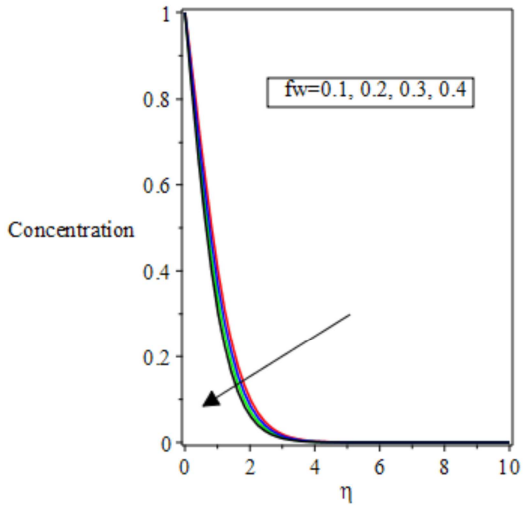

Figure 32. *Effects of fw on the Concentration profiles for Pr=0.72, λ=1, Ec=2, Ra =2, Q =2, Du = 2, = 0.1, Sr =2, Sc = 0.5, $k_1 = 0.1$, Gr =0.1, Gm =0.1, M_b =0.1 and $M_s = 0.1$.*

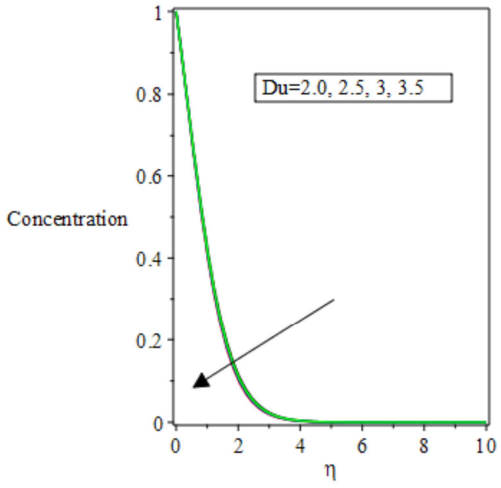

Figure 33. *Effects of Du on the Concentration profiles for Pr=0.72, λ=1, Ec=2, Ra =2, Q =2, n=5, Sr =2, Sc = 0.5, fw = 0.1,* $k_1 = 0.1$*, Gr =0.1, Gm =0.1,* M_b *=0.1 and* $M_s = 0.1$*.*

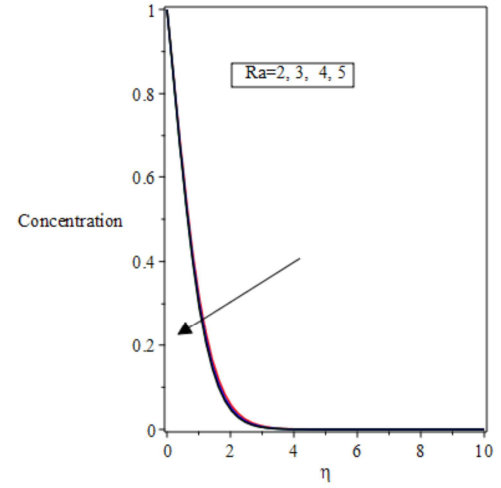

Figure 34. *Effects of Ra on the Concentration profiles for Pr=0.72, λ=1, Ec=2, Q =2, Du = 2, = 0.1, Sr =2, Sc = 0.5, fw = 0.1,* $k_1 = 0.1$*, Gr =0.1, Gm =0.1,* M_b *=0.1 and* $M_s = 0.1$*.*

6.3. The Effects of Varying Parameters on the Concentration Profiles

The concentration boundary layer behaviour as the parameters are changing is shown in Figures 24-33. Figure 27 reveals the influence of the magnetic parameter at the surface (M_s) on the concentration profile. It is realized that, increasing values of (M_s) increases the concentration profile. This is being validated in from results obtained in Golbert *et al*. [34]. Figures 29 and 24 describe the influence of Sc and Pr respectively on the species concentration. It is observed that increasing the Sc and Pr decrease the species concentration within the boundary layer. The lower the Schmidt number, the lower the mass diffusivity. This explains the decrease of the thickness of boundary layer concentration when Sc increases. The concentration boundary-layer thicknesses increase with increasing values of the buoyancy parameter in figure 31. Figure 32 demonstrates the ramification of *fw* on the concentration profile. It is seen that increasing values of suction, the concentration boundary layer thickness reduces. The outcomes of radiation parameter, Ra on the temperature outline are in figure 34. The temperature decreases when the radiation parameters are high. This is an enhancement of the thermal radiation thereby causing the convection moment in the boundary to increase. This decrease in the concentration distribution disperses away largely due to an increase in a temperature gradient.

In Figures 30 and 33, it is observed that an increase in Sr increases the concentration boundary layer thickness while little or no effect was observed with an increase in Du, respectively.

7. Conclusion

A steady MHD mass and heat flow in viscoelastic fluids pass a magnetized stretching plane surface with suction have been investigated. The modelled governing equations are transformed using the similarity analysis to ordinary differential equations. The transformed fourth-order ODES are further reduced to first-order ODEs by reduction order technique and solved numerically using the fourth order Runge-Kuta algorithms implemented in Maple 19 software. The following conclusions are drawn from the outcome of the results:

i. The induced Lorenz force and suction made the local skin friction to increase and deteriorate when the buoyancy forces, radiation, and viscoelastic parameter go up.
ii. The heat source parameter, suction enhances the heat transfer rate and reduces with radiation.
iii. The effect of M_b is seen to decrease the fluid flow but with an opposite effect on thermal boundary layer.
iv. The effect of increasing the buoyancy parameter has also been seen to reduce both the thermal and concentration boundary-layer thicknesses.
v. The effects of increasing Sr or decreasing Du tend to decreases the velocity and temperature profiles while enhancing the concentration distribution.

Nomenclature

u, v, w	velocity components in x, y and z axes (m/s)
B_0	Applied magnetic field (Wb/ m^2)
t	time (s)
T_w	Wall temperature (K)
U_0	Characteristic velocity (m/s)
C	Concentration (kg $/m^3$)
G	Acceleration due to gravity (m/s^2)
T	Temperature of the Casson fluid (K)
η	dimensionless similarity variable
f(η)	dimensionless similarity function
θ(η)	Dimensionless temperature
q_r	Radiation flux distribution in fluid (W/m^2)
Nu	Nusselt number
Sh	Sherwood number
K	Thermal conductivity of the fluid (W/m/K)
Pr	Prandtl number

$q^{\cdot}$	Volumetric heat generation(w)
M_s	magnetic parameter at the surface
M_b	magnetic parameter at the bulk
Br	Brinkmann parameter
k_1	Viscoelastic parameter
Du	Dufour parameter
Sr	Soret parameter

Greek Symbols

P	Fluid density (kg/m^3)
H	Similarity variable
Λ	Internal heat generation parameter
Σ	Electrical conductivity of fluid (m^2/s)
A	Thermal diffusivity
N	Kinematic viscosity (m^2/s)
$\boldsymbol{\psi}$	Stream function, (m^2 /s)
M	Fluid viscosity (kg/m/s)
β_T	Thermal coefficients (1/K)
β_C	Solutal expansion coefficients (1/kgm^3)

Conflict of Interest

The authors declared that they have no competing interest.

References

[1] Andersson, H. I. MHD flow of a viscoelastic fluid past a stretching surface, Acta. Mech. 95 (1992) 227–230.

[2] Abel, S. M., Sanjayanand, E. and Nandeppanavar, M. N.. Viscoelastic MHD flow and heat transfer over a stretching sheet with viscous and ohmic dissipations, *Communications in Nonlinear Science and Numerical Simulation,* 13, 2008, 1808-1821.

[3] Hsiao, K. L., "Viscoelastic fluid over a stretching sheet with electromagnetic effects and nonuniform heat source/sink", Mathematical Problems in Engineering, 2010, 14.

[4] Makukula, Z. G., Sibanda, P. and Mosta, S. S. "On new solutions for heat transfer in a viscoelastic fluid between parallel plates, *International Journal of Mathematical Models and Methods in Applied Sciences*, 4 (4), (2010) 221-230.

[5] Ghosh, K. S. and Shit, G. S. "Mixed convection MHD flow of viscoelastic fluid in a porous medium past a hot vertical plate", World Journal of Mechanics, 2, (2012) 262-271.

[6] Shehzad, S. A., Hayat, T. and Alsaedi, A. "MHD three-dimensional flow of viscoelastic fluid with thermal radiation and variable thermal conductivity", Journal of Central South University, 21, (2014), 3911-3917.

[7] Abel, M. S. and Mahesha, N., "Heat transfer in MHD viscoelastic fluid flow over a stretching sheet with variable thermal conductivity, non-uniform heat source and radiation", Applied Mathematical Modelling, 32, (2008) 1965-1983.

[8] Prasad, K. V., Pal, D. and Umesh, N. P. V. and Rao, "The effect of variable viscosity on MHD viscoelastic fluid flow and heat transfer over a stretching sheet", Communications in Nonlinear Science and Numerical Simulation. 15, (2010) 331-344.

[9] Cortell, R. (2014), "MHD (magneto-hydrodynamic) flow and radiative nonlinear heat transfer of a viscoelastic fluid over a stretching sheet with heat generation / absorption", Energy, 74, 869-905.

[10] Hayat, T., Ashraf, M. B., Alsulami, H. and Alhuthali, M. S. "Three-dimensional mixed convection flow of viscoelastic fluid with thermal radiation and convective conditions", PloS One, 9 (3), (2014), 3911-3917.

[11] Shuaib, H., Gul, T., Khan, M. A., Islam, S., Nasir, S. and Shah, Z. "Heat transfer and Unsteady MHD flow of third grade fluid past on vertical oscillating belt", Journal of Applied Environment Science, 5, (2015) 25-34.

[12] Abel, S., Prasad, K. V. and Mahaboob, A. "Buoyancy force and thermal radiation effects in MHD boundary layer viscoelastic fluid flow over continuously moving stretching surface", International Journal of Thermal Science, 44, (2005) 465-476.

[13] Chinyoka, T. and Makinde, O. D. (2012), "Unsteady hydromagnetic flow of a reactive variable viscosity third-grade fluid in a channel with convective cooling", International Journal for Numerical Methods in Fluids, 69, 353-365.

[14] Narayana, M., Gaikwad, S. N., Sibanda, P. and Malge, R. B. (2013), "Double diffusive magnetoconvection in viscoelastic fluids", International Journal of Heat and Mass Transfer, Vol. 67, pp. 194-201.

[15] Han, S., Zheng, L., Li, C. and Zhang, X. (2014), "Coupled flow and heat transfer in viscoelastic fluid with Cattaneo-Christov heat flux model", *Applied Mathematics Letters*, 38, 87-93.

[16] Rostami, B., Rashidi, M. M., Rostami, P., Momoniat, E. and Freidoonimehr, N. (2014), Analytical Investigation of Laminar Viscoelastic Fluid Flow over a Wedge in the Presence of Buoyancy Force Effects, Hindawi Publishing, doi: 10.1155/2014/496254:11.

[17] Sheikholeslami, M., Ganji, D. D., Bandpy-Gorji, M. and Soleimani, S. (2014), "Magnetic field effect on nanofluid flow and heat transfer using KKL model", Journal of Taiwan Institute of Chemical Engineers, Vol. 45, pp. 797-801.

[18] Khan, J. A., Mustafa, M., Hayat, T. and Alseadi, A. (2015), "Numerical study of cattaneo-christov heat flux model for viscoelastic flow due to an exponentially stretching surface", PloS One, Vol. 10 No. 9, e0137363.

[19] Abdou, M. M., El-Zahar, E. R. and Chamka, A. J. (2015), MHD mixed convection stagnation-point flow of a viscoelastic fluid towards a stretching sheet in a porous medium with heat generation and radiation, *Canadian Journal of Physics,* 93 (5), 532-541.

[20] Mohammad M. R., Mohamed A., Behnam R., Peyman R., and Gong-Nan X. (2015). Heat and mass transfer for MHD viscoelastic fluid flow over a vertical stretching sheet with considering Soret and Dufour effects, *Mathematical Problems in Engineering,* http://dx.doi.org/10.1155/2015/861065.

[21] Prashant G. M., Pushpanjali G. M., Subahas A., Sergie S. S. (2016). Heat Transfer in MHD Mixed Convection Viscoelastic Fluid Flow over a Stretching Sheet Embedded in a Porous Medium with Viscous Dissipation and Non-uniform Heat Source/Sink, *Procedia Engineering* 157: 309-316, DOI: 10.1016/j.proeng.2016.08.371.

[22] Abbasi, F. M., Mustafa, M., A Shehzad, S., Alhuthali, M. S. and Hayat, T. (2016), "Analytical study of Cattaneo-Christov heat flux model for a boundary layer flow of Oldroyd-B fluid", *Chinese Physics B*, 25 (1), 014701.

[23] Ganesh K. K., Gireesha B. J., Manjunatha S. And Rudraswamy N. G. (2017). Effect of nonlinear thermal radiation on double-diffusive mixed convection boundary layer flow of viscoelastic nanofluid over a stretching sheet, *International Journal of Mechanical and Materials Engineering* 12 (1): 18, DOI: 10.1186/s40712-017-0083-5.

[24] Gangadhar, K., Kumar, C. S., S Ibrahim, M. and Lorenzini., G. (2018), "Effect of viscous dissipation on upper - convected Maxwell fluid with cattaneo-christov heat flux model using spectral relaxation method", Scientific, Net, 388, 146-157.

[25] Kashifi, A. A., M Baig, M. and Hussain, M. (2018), "Influences of magnetic field in viscoelastic fluid", Int. Journal of Nonlinear Analysis and Applications, 9 (1), 99-109.

[26] Kumar B., Gauri S. S, Raj N. and Chamkka A. J. (2019). Outlining the impact of induced magnetic field and thermal radiation on magneto-convection flow of dissipative fluid, *International Journal of Thermal Sciences* 146 (4): 106101.

[27] Menni, Y., Chamkha, A. J., Massarotti, N., Ameur, H., Kaid, N. and Bensafi, M. Hydrodynamic and thermal analysis of water, ethylene glycol and water-ethylene glycol as base fluids dispersed by aluminum oxide nano-sized solid particles, *International Journal of Numerical Methods for Heat & Fluid Flow*, 30 (9), (2020), 4349-4386.

[28] Ullah, A., Shah, Z., Kumam, P., Ayaz, M., Islam, S. and Jameel, M. (2019). Viscoelastic MHD nanofluid thin film flow over an unsteady vertical stretching sheet with entropy generation, *Processes,* Vol. 7 No. 262.

[29] Jafar, A. B., Shafie, S. and Ullah, I. (2019), Magnetohydrodynamic boundary layer flow of a viscoelastic fluid past a nonlinear stretching sheet in the presence of viscous dissipation effect", Coating, Vol. 9 No. 490.

[30] Shojaei, A., Amiri, A. J., Ardahaie, S. S., Hosseinzadeh, Kh. and Ganji, D. D. (2019), "Hydrothermal analysis of Non-Newtonian second grade fluid flow on radiative stretching cylinder with Soret and Dufour effects", Case Studies in Thermal Engineering, Vol. 13 No. 100384.

[31] Gholinia, M., Gholinia, S., Hosseinzadeh, K. and Ganji, D. D. (2018), "Investigation on ethylene glycol Nano fluid flow over a vertical permeable circular cylinder under effect of magnetic field", Results in Physics, 9, 1525-1533.

[32] Ogunseye, H. A., Sibanda, P. and Mondal, H. (2019). On MHD mixed convective stagnation point flow of an Eyring-Powell nanofluid over a stretching cylinder with thermal slip conditions, *Journal of Central South University*, 26, 1172-1183.

[33] Rahimah M., Noraihan A. R., Abdul R. M. K., Sharidan S. (2020). Mixed convection flow of viscoelastic nanofluid past a horizontal circular cylinder in presence of heat generation *Malaysian, Journal of fundamental and applied sciences* 16 (2): 166-172.

[34] Golbert A, Seini, IY and Rabiu M. (2021). Heat Transfer in a Magnetohydrodynamic Boundary Layer Flow of a Non-Newtonian Casson Fluid Over an Exponentially Stretching Magnetized Surface. Journal of Nanofluids. 10, 172-185.

[35] Etwire, CJ, Seini, IY, Rabiu, M, Makinde, OD, (2021). On the Flow of Oil-Based Nanofluid on a Stretching Permeable Surface with Radiative Heat Transfer and Dissipative Energy. Diffects and Difussion Furum. 409, 1-16.

[36] Sulemana, M, Seini, IY, (2021). Time-Dependent Hydromagnetic Boundary Layer Flow across a Vertical Surface in a Porous Media with Internal Heat Generation. Engineering Fluid Flows and Heat Transfer Analysis II. Defects and Diffusion. 409, 17-38.

[37] Seini, IY, Aloliga, G, Ziblim, B, Makinde, OD, (2020). *Boundary layer flow of casson fluid on exponentially stretching porous surface with radiative heat transfer*. Diffusion Foundations. 26, 112-125.

[38] Etwire, CJ, Seini, IY, Rabiu, M, Makinde, OD, (2019). *Impact of thermophoretic transport of Al_2O_3 nanoparticles on viscoelastic flow of oil-based nanofluid over a porous exponentially stretching surface with activation energy*. Engineering Transactions. 67 (3), 387 – 410.